Carbon Nanotube–Magnetite Composites, With Applications to Developing Unique Magnetorheological Fluids

Stephen Samouhos[1]
e-mail: stratos@mit.edu

Gareth McKinley

Hatsopoulos Microfluids Laboratory,
MIT,
Department of Mechanical Engineering,
77 Massachusetts Avenue,
Cambridge, MA 02139

The development of carbon nanotube (CNT) based technology is limited in part by the lack of effective bulk methods for precisely manipulating and aligning nanotubes at the very fine scale. Moreover, the innate hydrophobic and inert nature of the CNT surface limits their compatibility with aqueous systems and flexibility for surface chemistry functionalization. This paper assesses the variety of methods developed to couple magnetically susceptible components such as ferromagnetic material with CNTs in order to overcome these limitations. In addition to reviewing the past 16 years of relevant literature, our own methods for noncovalent surface coating of CNT's with magnetite nanoparticles are described. The application of such composites is then explored within the framework of a magnetorheological (MR) fluid. It is found that the addition of magnetite nanoparticles to a MR fluid enriches the available MR response, resulting, in some cases, in an increased sedimentation stability, larger saturation critical stresses, and faster response to time varying magnetic fields. Finally, our own composite based MR fluid is discussed, and shown to possess a field dependent response that is a hybrid between that observed in ferrofluids and conventional MR fluids. [DOI: 10.1115/1.2436581]

Keywords: carbon nanotube, magnetite nanoparticles, magnetorheological, nanocomposite

Introduction

Carbon nanotubes (CNT) have received a tremendous amount of attention due to their unique and highly desirable electrical, thermal, and mechanical properties [1]. A variety of potential CNT applications exist, however, technology development is in part hampered by the lack of effective means for manipulating these materials at very fine scales [1]. Magnetic actuation of CNTs offers a potentially simple means for exerting this necessary control; however success is dependent on the ability to magnetize the CNT. Due to the absence of any natural CNT paramagnetism [1], their magnetization is only accomplished through hybridization with other magnetic materials, in particular cobalt, iron, nickel, and gadolinium. In this paper, we review the variety of methods demonstrated to couple magnetic materials with CNTs, as well as the performance of the composite as a magnetorheological fluid.

There are three general approaches to creating a magnetic CNT composite; magnetic material can be encapsulated [2–7], incorporated within the walls [8–15], or deposited on the outer surface of the nanotube [16–18]. All three methods have been shown to impart some magnetic character to the nanotube. Each approach, however also modifies the nanotube in ways that may ultimately restrict the applications of the composite. Beyond these three material addition categories, methods can be further subdivided into chemical and physical techniques that result in magnetic CNT composites. Physical additions include most of the processes in which material is encapsulated or imbibed by the nanotube, and as such, the majority of the molecular structure is kept intact. Wall embedding and outer surface decoration generally require, or induce some change in the wall or outer surface chemistry.

Filling Techniques for Composite Formation

The earliest methods to create magnetic CNTs followed from the work of Ajayan and Iijima in 1993 [3], who successfully demonstrated the oxidative cleavage of CNT end caps and subsequent filling with nonmagnetic liquid metals. Approaches derived from the work of Ajayan and Iijima relied upon filling a tube with magnetically susceptible liquids. Initially this was accomplished by selectively oxidizing the ends of a fully formed nanotube, and then using capillary suction to imbibe a volume of liquid metal into the freshly opened tube [2,3]. This two step process was executed by first depositing metallic nanoparticles onto a pristine nanotube outer surface, and then heating the composite material in air to beyond the melting temperature of the metal. The heating process both oxidized the tube end caps, as well as liquefied the metal. With the advent of techniques for creating vertically aligned, open ended CNTs [19], several other filling methods were also established.

In 2002, Bao et al. [4] showed that electrodeposition could be used to directly create continuous wires of cobalt within vertical nanotubes on an alumina template. Leonhardt et al. [5] provides a review of analogous chemical vapor deposition techniques for creating metal nanowires of iron, nickel, and cobalt within nanotubes. In a slightly different approach, Wu et al. [7] demonstrated that an aqueous solution of Fe and Ni ions could be drawn into a CNT and, through wet chemistry, form Fe–Ni alloy nanoparticles within the CNT. Finally, Korneva et al. [6] in 2005, also showed that an aqueous suspension of magnetic nanoparticles could be drawn by capillary suction, directly into an open ended nanotube. Subsequent evaporation of the solvent resulted in nanotubes loaded with magnetic nanoparticles. Most of these processes involve physical deposition, with minimal molecular modification of the CNT. In contrast, wall embedding and surface decoration generally involve significant chemical alterations of the CNT surface.

[1]Corresponding author.

Contributed by Fluids Engineering Division of ASME for publication in the JOURNAL OF FLUIDS ENGINEERING. Manuscript received June 28, 2006; final manuscript received December 5, 2006. Assoc. Editor: Dennis Siginer.

Wall Embedding and Surface Decoration Pathways

One of the earliest chemical additions of magnetic material to CNTs, performed by Lafdi et al. in 1996, was accomplished through cobalt doping of the graphite electrode used in arc-discharge CNT synthesis [10]. The CNTs subsequently produced from the doped electrode possessed walls that were infused with cobalt nanoparticles. Alternatively, Rao et al. [11] used pyrolitic synthesis, catalyzed by ferrocene, to form CNTs that had a magnetic nanoparticle embedded within the tube, at the catalyst anchoring point. Whereas Lafdi [10] was able to distribute the cobalt along the entire length of the tube, this latter approach could inherently only place a nanoparticle at one point. The methods employed by Rao were expanded in 2000 and 2001, by Liu et al. [12,13], and Zhang [15], respectively. Barnhart [14] provides a more complete review of the chemical and physical effects of metal atom inclusions within CNT walls, as well as the synthesis pathways leading to such composites.

In 2005, Bottini et al. [20] showed that multiwalled CNTs could be covalently decorated with silica nanoparticles. The protocol required a long oxidation step to carboxylate the surface, after which various nanoparticle precursor groups could be attached to the induced surface defects. Extended oxidation in concentrated nitric acid was necessary in order to stud the largely inert pristine CNT surface with reactive carboxylic groups. The protocol stems from an established method of using moderate etching periods in strong oxidizers to create nanotubes of uniform and predictable length, with minimal aberrations of the outer surface [21]. By dramatically extending the etch time, Bottini et al. increased the surface concentration of carboxyl group defects. As evidenced by transmission electron microscope (TEM) imaging of the composite material, the defect concentration was not sufficient to support total outer surface coverage by silica nanoparticles.

Georgakilas et al. [16] used a slight variation of this method in that same year, to stud the outer wall surface with magnetite. Utilizing π bond stacking, carboxylic defect groups on the CNT surface were bonded to a pyrene-bearing magnetite nanoparticle, with an average diameter of 25 nm. As with other approaches that utilize surface defects, the coating process resulted in only partial coverage of the tube. Similar work was also presented in 2005 by Stoffelbach et al. [18] for decorating the outer surface with magnetite, and also in 2006 by Cao et al. [22]. Finally in 2005, Wu et al. [23] showed that by a similar process, nickel–iron alloy nanoparticles could be grown on the outer surface of the nanotube. In their protocol, the nanotube is again subjected to a prolonged oxidative bath in boiling nitric acid, which results in the formation of carboxylic surface defects. These imperfections provide the point of attachment for subsequent nanoparticle precursors. In all cases, the density of surface defects is insufficient for complete coverage of the nanotubes by magnetic materials.

Selection Considerations for CNT–Nanoparticle Hybridization Techniques

External magnetic coatings offer the capability of magnetic actuation as well as continued CNT surface functionalization [22]. As the pristine CNT surface is chemically inert, localized magnetic surface groups, attached to the CNT, can provide points of attachment for materials that would otherwise not adhere to the CNT. Along those lines, the utility of such coatings, either in magnetic control or surface functionalization, is limited by the extent of surface coverage. One of the goals of our work is to develop magnetite surface coating techniques that result in complete coverage of the CNT.

The scientific interest in developing and reviewing the current techniques for nanotube-to-nanoparticle hybridization is ultimately driven by the needs of the design engineer who wishes to create precise multiscale systems. Our particular work is devoted to hybridization techniques that do not destroy the innate surface chemistry of either particle.

Choosing amongst the existing art is dictated mostly by chemistry and application criteria of the hybrid materials. For a generic magnetic application, it may be sufficient to rely solely upon the incorporation of the magnetic catalyst used during tube synthesis. This simple approach may prevail for long tubes that eventually only need one magnetic anchoring point. On the other hand, many synthetic processes are followed by a cleavage etch that would create tube segments with no magnetic character. Such situations can be resolved either by post-etch addition steps of either physical or chemical nature, or impregnation of the tube wall with magnetic particles during growth. Tube filling is another option that offers certain advantages to surface engineering, and can also be performed in situ with tube growth or post-cleavage etch. Applications that demand preservation of the outer tube surface chemistry should look to tube filling techniques. These same methods have generally also resulted in superior addition of magnetic character to the nanotubes.

Other than chemical and design criteria, production cost is certainly important for choosing a hybridization technique. Surface additions stem from the acid etch induced carboxylation of the CNT, which is a relatively low-cost process step. The oxidation of the surface provides reaction sites that can be harnessed by numerous chemical means to deposit materials on the CNT surface. In general, these post-synthesis steps are easy to apply, and can be performed by any laboratory. In contrast, the deposition techniques for in situ tube filling during synthesis require a reaction chamber set up for the particular chemical vapor deposition (CVD) process. Most CNT synthesis laboratories already have such utilities, but groups who purchase CNT might have to consider the added cost of that process in comparison to surface chemistry methods. The development of simple capillary suction methods for filling CNT represents a significant departure to this classical CVD paradigm, creating a low-cost, highly effective tube filling procedure. Our efforts to develop simple, analogous low-cost surface encapsulation techniques that preserve the CNT outer surface chemistry would also provide additional options for the design engineer.

Method for Total Encapsulation of Carbon Nanotubes by Magnetite

A surface-preserving encapsulation procedure seemed feasible through noncovalent bonding between nanoparticles and tubes. In the absence of a chemical reaction or electrostatic bonding with surface defects, such a process could most likely proceed from the minimization of the van der Waals potential between the spherical nanoparticles and cylindrical nanotubes [24,25]. Kirsch [25] has shown that for certain geometric and material parameter values, the van der Waals attraction is greatest between a sphere and cylinder than for either species to a neighbor of its own kind. In reality, minimal surface defects always arise from the brief oxidative bath, as prescribed by Liu et al. [21], used to cut CNTs to a desired length. In the case of defects, electrostatic interactions introduce random points of attachment that do not usually support full tube encapsulation. Not having to depend on defect anchor points, the desired noncovalent bonding mechanism may result in full surface coverage.

The CNTs used to explore this technique were acquired from NanoLabs (Newton, MA), who carried out the ferrocene pyrolitic synthesis of 30 nm outer diameter stock multiwalled CNTs. The synthesis was followed by a 3 h concentrated nitric acid reflux etch, performed by NanoLabs, that cleaved the stock material into 5 μm long, open-ended segments. TEM inspection coupled with the low aqueous miscibility confirmed that the outer tube surface acquired minimal carboxylation defects during the etch. No further oxidation steps or chemical treatments were employed after the etching bath.

To explore the noncovalent bonding mechanism, 10 ml of an organic ferrofluid (EFH-1, Ferrotec, Nashua, NH), and a water-based ferrofluid (MSG-W11, Ferrotec, Nashua, NH) were added

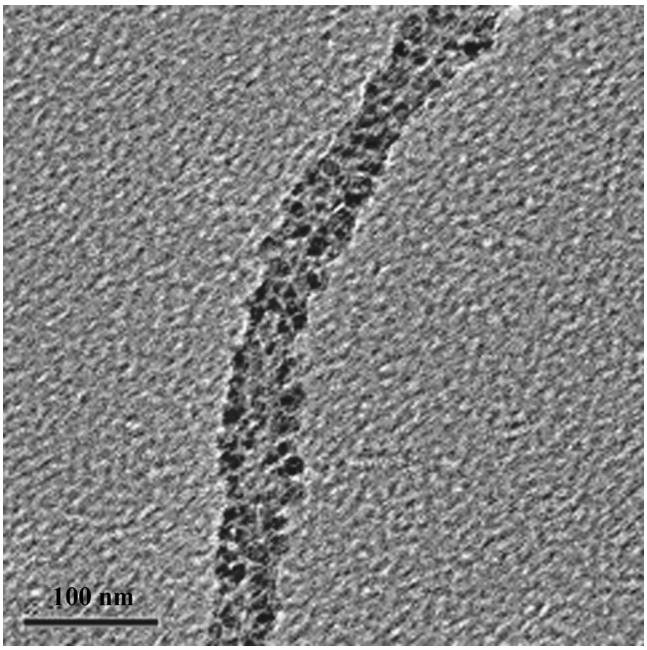

Fig. 1 TEM of organic ferrofluid nanoparticles bound to a CNT

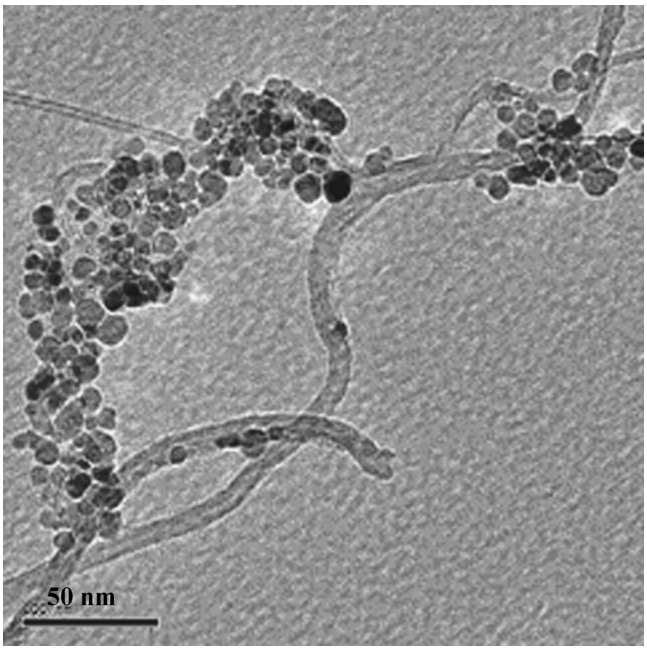

Fig. 2 TEM of aqueous ferrofluid nanoparticles excluding CNTs

drop wise to separate Petri dishes each containing 1.0 g dry CNT samples. Both ferrofluids were constituted of 10 nm magnetite nanoparticles, coated with an appropriate surfactant, and loaded to 6% volume fraction in their respective carrier liquid. As expected from prior miscibility experiments, the CNTs exhibited strong hydrophobicity, and the aqueous ferrofluid did not spontaneously wet the nanotubes. Conversely, the CNTs were immediately wet by the organic ferrofluid. The contents of each dish were mixed with a glass rod, and then washed with excess ethanol into 45 ml plastic tubes, without any sonication. The tubes were shaken vigorously to further mix the materials. The tube contents were separately washed with excess ethanol, and then excess kerosene, through a vacuum filtration system. In both cases, a reddish brown filtrate ensued, with a dark pink colored solid remaining on the filter paper.

The filtrate was discarded, and the filter paper contents were washed with ethanol back into glass vials for storage. Figures 1 and 2 show TEM micrographs (100 kV acceleration potential) of both the oil and water based ferrofluid reaction products in ethanol, following 3 h of sonication.

The magnetite particle and CNT diameters can be estimated from the TEM images as approximately 10 nm and 30 nm, respectively. These values match the quoted sizes given by the manufacturers. The initial hydrophobic interaction and poor miscibility between aqueous ferrofluid and CNT may have foretold the results shown in Fig. 2. The aqueous ferrofluid particles generally agglomerate with themselves, and occasionally attach to the surface of the CNT. The sporadic surface deposition may be attributed to the presence of a low concentration of carboxyl surface defects initiated by the oxidation etch. These defects facilitate electrostatic bonding with the charged surfactant group of the aqueous ferrofluid magnetite particle. In stark contrast, the organic ferrofluid appears to have fully coated the entire CNT. This image is reproduced in several other TEM micrographs, and indicates that our process results in complete CNT coating by magnetite nanoparticles. Based on the conditions of the experiments, noncovalent bonding due to van der Waals attraction or surfactant–CNT surface affinity has produced hybrids with high surface coverage. Moreover, the composite products of the organic reaction can be stabilized by a surfactant such as CTAB, or SDS and show satisfactory sedimentation stability in water, up to 0.1% volume fraction. The composite material alone shows higher stability against sedimentation in organic media without the aid of any surfactants.

The scanning electron microscope (SEM) image in Fig. 3 shows a larger object, comprised of several of these magnetite/CNT composites. Considering the dimensions of an individual strand, as shown in the TEM above, this SEM suggests that several composite strands can braid or envelope each other to form a bamboo structured micron-sized cylinder.

Figures 4 and 5 present static snapshots of the alignment of these braided composite strands to a lateral and normal induction field of 20 mT. The composite is clearly manipulated by the field to remain parallel with the field lines. There is likely a critical size, or number of strands per cylindrical agglomerate, that is indicative of steric and perhaps magnetic interactions between individual composite tubes. This saturation size is supported by the observation that Figs. 3–5 show a large number of these agglomerate braids all with roughly 2.5 μm diameter and 20–30 μm in length. The manufacturer's quoted dimensions for the nanotubes are 30 nm diameter, by 5–20 μm long; considering that a mag-

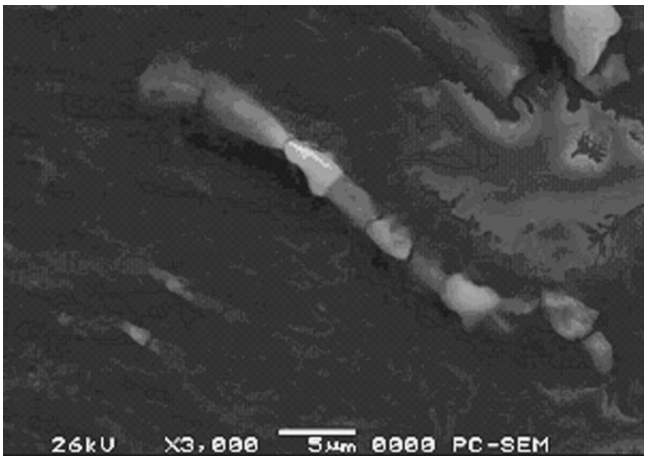

Fig. 3 SEM of bamboo structured ferrofluid nanoparticle–CNT composite

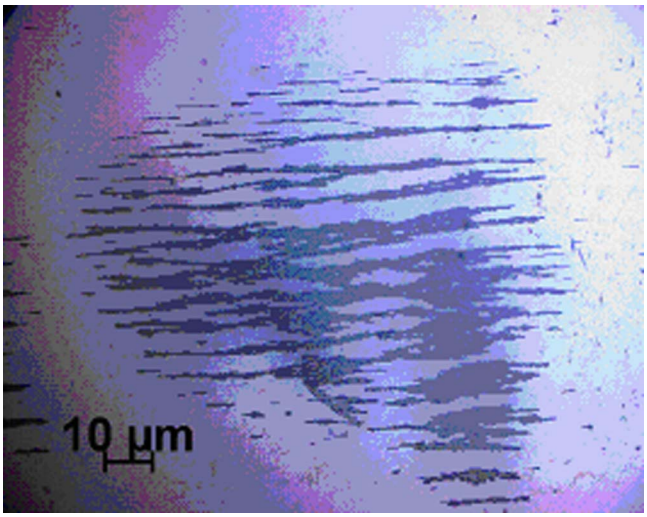

Fig. 4 Micrograph of composite filaments aligned by 20 mT field applied parallel to the page

netic coat increases the outer diameter to 60 nm, these braided agglomerates are comprised of roughly 40–50 individual strands.

Correa-Duarte et al. [26] also achieved complete coverage with magnetite through a noncovalent bonding mechanism based on polymer wrapping and layer-by-layer (LbL) electrostatic self-assembly. Poly(sodium 4-styrene sulfonate) chains were driven to wrap around the CNT via hydrophobic interactions, thereby encapsulating the CNT in a negatively charged polymer coat. The polymer surface charges then acted as anchors for the subsequent deposition of magnetic nanoparticles via LbL, and total surface coverage ensued. Pu and Jiang [27] also attempted surface coating via extended oxidation to create carboxyl defects on the CNT surface. These defects served as nucleation sites in the subsequent chemical synthesis of magnetite from ferrous and ferric salts. This approach resulted in the formation of a 10-nm-thick shell of magnetite surrounding the CNT. TEM analysis, however, shows a shell that only covers certain portions of the CNT, as opposed to the total surface coverage wrought by our noncovalent bonding. In contrast to other carboxylation-based methods, however, which result in only particle decoration of the CNT surface, Pu and Jiang were successful in producing continuous magnetite shells on the CNT surface, albeit without total surface coverage.

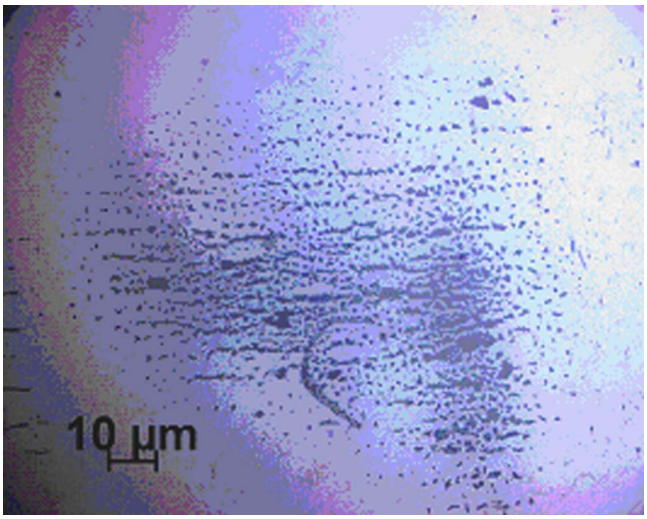

Fig. 5 Micrograph of composite filaments aligned by 20 mT field applied normal to the page

Sedimentation Stability of CNT/Magnetite Composite Based MR Fluids

Part of the motivation for creating a CNT/magnetite composite stems from the goal of creating a magneto-rheological (MR) fluid with increased sedimentation stability. The density of the magnetite/CNT composite formed by our protocol was approximately 1.8 g/cm^3, which is less than a quarter of that of carbonyl iron, $Fe(CO)_5$, a material commonly used to form particles for MR fluids. By comparing the buoyancy of a particle against the viscous drag experienced as it falls within a fluid, the sedimentation velocity may be expressed by [28]

$$V_0 = 2(\rho_s - \rho_f)ga^2/9\eta \tag{1}$$

where V_0 is the sedimentation velocity; ρ_s and ρ_f are the particle and fluid densities respectively; a is the particle radius; η is the viscosity of the fluid; and g is the gravitational acceleration. The difference in density between a 1-μm-diameter CNT/Fe_3O_4 composite particle and 1-μm-diameter iron oxide particle should result in a 17-fold reduction in the sedimentation velocity of the composite as compared to iron oxide particles, dispersed in water. Moreover, at high enough volume fractions (above 10%), the elongated cylindrical shape of the braided composite particles should also provide sedimentation stability via the formation of a percolated network. Pu and Jiang created a composite with similar density and cylindrical geometry, and found that the sedimentation stability of their CNT/magnetite composites dispersed in water increased with increasing volume fraction. Their result was attributed to the formation of a percolated support structure that prevented sedimentation.

The sedimentation stability of MR fluids has been a continual problem in the development of MR fluid technology [29,30]. The combination of hollow, lighter weight CNTs with superparamagnetic [31] magnetite nanoparticles can lead to a unique MR fluid that does not suffer from sedimentation limitations. The improved stability may be realized through both the use of composite materials with lower mass densities as well as particle geometries such as elongated cylinders that form percolated networks. The success of these novel MR fluids, however is contingent upon the preservation of the field-dependent critical stress and modulus seen in conventional iron oxide and carbonyl iron based MR fluids [32–35].

Magnetorheological Fluids and Ferrofluids

Conventional MR fluids date back to their discovery in 1948 by Rabinow [36]. They followed as a natural magnetic analog to the electro-rheological fluid patented by Winslow [37] in 1947. Depending on the desired effect, the fluids are surfactant-stabilized suspensions of either dielectric, or paramagnetic micron sized particles, dispersed in a carrier liquid. Ferrofluids [31] are another family of magnetically active liquids, whose surfactant stabilized particle constituents are 10–20 nm in size, and consist of single domain, permanently magnetized magnetite. Consequently, the response of a ferrofluid to a magnetic field is markedly different from that of an MR fluid [31].

MR fluids consisting of 1 μm carbonyl iron particles, at 30% volume fraction, have a maximum critical stress in the range of 10–100 kPa for applied induction fields near 0.2 T [32,34]. The zero-shear-rate viscosity, which persists until the critical stress is surpassed, may exceed 1 MPa s. In contrast, the electro-rheological (ER) effect provides critical stresses typically no greater than 1 kPa, at fields near 1 kV/mm. This performance limitation is imposed by impurities within the carrier liquid, oxide layers on the dispersed particles, and the dielectric breakdown voltage of the ER suspension carrier fluid. Analogously, the MR effect is limited by the saturation magnetization of the constituent

magnetic material. Coating techniques similar to the surface decoration methods we have discussed above have also been used to overcome these ER limitations by creating a high dielectric constant suspension of urea-coated barium titanate oxalate nanoparticles, suspended in silicone oil. The resulting ER fluid exhibits an unprecedented 130 kPa yield stress without dielectric breakdown [38].

MR fluids show an apparent viscosity that is dependent on the applied magnetic field, shear stress, particle volume fraction, and carrier viscosity [35]. With the application of a magnetic field at values below the saturation value for the paramagnetic material, a magnetic dipole results according to

$$\vec{m} = \tfrac{4}{3}\pi a^3 \mu_0 \chi \vec{H} \tag{2}$$

where $\vec{m}$ is the particle polarization; a and χ are the particle diameter and dimensionless susceptibility, respectively; and μ_0 and H are the free space permeability and applied field, respectively [35]. The induced dipoles interact with one another to form particulate aggregates whose size grow with the square root of elapsed time (measured from the onset of the magnetic field) [39]. The particle aggregates grow into longer bundles, and eventually into threads extending along the magnetic field lines. Eventually, these threads coarsen due to lateral attraction and form crystalline pillars of magnetized particles [34,40]. The formation of aggregates is opposed by Brownian dispersion, and as such the potential for field induced aggregation versus Brownian dispersion can be expressed in terms of a governing dimensionless parameter, often referred to as a coupling coefficient

$$\lambda = \frac{\pi(\mu_0 \chi H)^2 a^3}{18 k_B T} \tag{3}$$

where the parameters T and k_B are the temperature and Boltzmann constants, respectively [35]. For the case $\lambda \gg 1$, aggregation is highly favored, and at $\lambda \ll 1$, dispersion is favored. The case of small λ is used as a design parameter for the creation of ferrofluids, or stable dispersions of superparamagnetic nanoparticles in organic and aqueous carriers [31], whereas $\lambda \gg 1$ commonly results in MR fluids [35]. Due to the presence of permanent magnetic material within ferrofluids, as opposed to the paramagnetic material typically found in MR fluids, the aggregation parameter for ferrofluids is calculated according to

$$\lambda = \frac{\mu_0 M_s H \pi a^3}{6 k_B T} \tag{4}$$

where $\mu_0 M_s$ is the remnant magnetization of the particle [31].

The reorganization of the MR fluid microstructure due to shearing comes via the interplay of hydrodynamic and magnetic forces. The ratio of these interactions within an MR fluid forms a second dimensionless parameter known as the Mason number [32,35,41] that governs the breakup of magnetic microstructure due to shear

$$\mathrm{Ma} = \frac{9\sigma}{2(\mu_0 \chi H)^2} \tag{5}$$

where the parameter σ is the applied shear stress. Alternate governing dimensionless parameters include a Péclet number (dimensionless time) formed by the ratio of shear rate to the Brownian diffusion time as well as the particle volume fraction. The Mason number (Eq. (5)), Péclet number, and coupling coefficient (Eqs. (3) and (4)) are interrelated via $\mathrm{Pe} \sim \mathrm{Ma} \times \lambda$. An analogous ferrofluidic Mason number can be constructed by the ratio of the applicable Peclet and aggregation parameters. In contrast to MR fluids, the field-independent rheological properties of ferrofluids reduce the utility of a ferrofluidic Mason number.

At low applied fields, where saturation effects are completely absent, the Maxwell magnetostatic stress accurately predicts that the yield stress σ_c within MR fluids is proportional to the square of the applied magnetic field [33]. As the field intensity is increased such that saturation begins to occur at the surface of the dipolar particles, the critical stress (σ_c) transitions to a weaker dependence on the applied field, and the elastic modulus (G) grows linearly with the applied field. Ginder et al. [33] were able to model this saturation effect and found analytical models for the critical stress and elastic modulus that accurately predicted the data for carbonyl iron MR fluids [33,42]

$$\sigma_c = \sqrt{6}\phi \mu_0 M_s^{1/2} H^{3/2} \tag{6}$$

$$G = 3\phi \mu_0 M_s H \tag{7}$$

where ϕ is the volume fraction. This saturation effect is amplified by the increased field density within the small gap between particles undergoing aggregation. At still higher fields that exceed the physical saturation magnetization of the magnetic material, the response becomes field independent and limited only by the saturation of the material and particle volume fraction

$$\sigma_c^{\mathrm{sat}} = 0.086 \phi \mu_0 M_s^2 \tag{8}$$

$$G^{\mathrm{sat}} = 0.3 \phi \mu_0 M_s^2 \tag{9}$$

In stark contrast to the performance of MR fluids, ferrofluids do not display a dramatic change in viscosity as a function of applied field [43]. There is a marginal change in fluid viscosity at very small shear rates with an applied field, but at high shear rates or strong applied fields, the apparent viscosity does not change. Moreover, an exceedingly small (if any) critical stress exists for the ferrofluid, irrespective of the applied field [31]. This difference in response between these two magnetically-active fluids results from the typical magnitudes of the λ parameter previously defined in Eqs. (3) and (4) for MR and ferrofluids, respectively; for $\lambda \ll 1$, as is the case with ferrofluids, persistent filamentous or tertiary aggregates cannot form even in strong magnetic fields. In the absence of such a microstructure, the ferrofluid does not exhibit a critical stress induced by a magnetic field [31]. A field dependent viscosity is observed in ferrofluids, but is attributed to the torque of a rotating magnetic field on the nanoparticles themselves [44]. Represented as an unsymmetric stress tensor within the continuum description of the ferrofluid, so called negative or zero fluid viscosities can be observed, and are a result of the rotating magnetic field [45,46]. In the absence of a magnetic field, the viscosity shows some shear thinning at high shear rates. The apparent viscosity is generally considered to be volume fraction dependent according to the Einstein relation in the dilute suspension limit [31]

$$\frac{\eta}{\eta_0} = 1 + \frac{5}{2}\phi \tag{10}$$

where η_0 is the nominal carrier viscosity, and η is the apparent viscosity of the suspension. Higher order terms can be included to account for volume fractions beyond the dilute limit [31]. Whereas MR fluids typically have volume fractions exceeding 30%, commercial ferrofluids do not extend beyond 10%.

Combined MR and Ferrofluids

Several approaches have been taken to improve the magnitude and speed of MR fluid response [29,47]. Of note are methods for increasing the field-on viscosity to attain a more solid-like response below the critical stress [48], as well as methods for decreasing the response time, or lag between fluctuating field and particle tracking [49], and finally increasing the critical stress via reducing the limitations imposed by magnetic saturation [50]. These methods tend to employ mixtures of both nano- and micro-sized magnetic material, which often has the additional benefit of increasing sedimentation stability [49–51].

Popplewell et al. [48] explored inverse MR fluids in 1995 to achieve some of these improvements. A commercial ferrofluid was used as the carrier liquid, with a suspension of 1 μm glass beads. It was found that application of a magnetic field induced

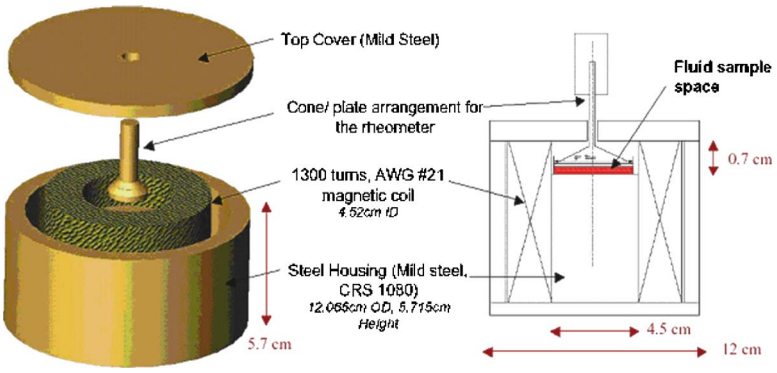

Fig. 6 Custom designed MR fixture for AR2000 rheometer

the formation of rudimentary glass bead columnar structures, and a typical MR response ensued, albeit with reduced critical stress. For bead volume fractions at 60%, and 36 mT induction field, the critical stress was about $\sigma_c \sim 20$ Pa, with an ensuing viscosity of 0.4 Pa s. Experiments were repeated with aluminum and iron parallel plates, and the iron geometry was found to produce a greater divergence in the zero shear rate viscosity. It was proposed that the lack of magnetic attraction between the aluminum geometry and ferrofluid provided a mechanism for slip and hence a reduction in the zero-shear rate viscosity. Owing to the paramagnetic nature of both the ferrofluid and iron, and the diamagnetic nature of aluminum, the ferrofluid magnetically adheres to the iron plate, and provides a more accurate measurement of the viscoplastic solid-like creep response below yield.

The limitations due to saturation and sedimentation were both explored by Chin et al. [50] in 2001. Building on prior work by Phule and Ginder [52] and Chen et al. [53], MR fluids comprised of micron sized carbonyl particles, interspersed with cylindrical nanoparticles of Co–γ–Fe_2O_3 and CrO_2, were created and shown to have a dramatically increased sedimentation stability and saturation critical stress. The critical stress enhancement was found to be a strong function of applied magnetic field, with an increase of 30% in a 64 mT field, versus less than 5% for a 16 mT field. This enhancement phenomenon was attributed to a shielding effect owing to the greater saturation magnetization found within cobalt materials as compared to carbonyl iron.

As was shown by Ginder et al. [33], saturation begins to limit the MR effect once the MR particles begin to experience localized saturation due to the increased field density within the thin gap between magnetic particles. By interspersing the gap with nanoparticles of higher magnetic saturation (cobalt materials can have nearly double the saturation of purely ferromagnetic species), the increasing field density can be distributed between MR particles and cobalt particles, where the greater saturation of the cobalt can shield the MR particles from reaching saturation. This shielding effect proposed by Ginder is less pronounced at lower fields, where neither the nanoparticles nor MR particles are near saturation. However, as the field strength increases, the saturation mitigated by the nanoparticles results in a greater interaction between MR particles, and hence stronger columnar structures and increased critical stress.

Based purely on nanoparticle MR fluids have also been explored independently by Kormann et al. [49]. Ferrite nanoparticle suspensions of roughly 30 nm diameter, and 60% mass fraction, were shown to behave as MR fluids. This is in stark contrast to ferrofluids with particle sizes only half the diameter, and volume fractions less than a sixth that value. At zero applied field there was only a small critical stress resulting from a percolated network, but as the field was increased to 0.4 T, the critical stress rose almost to $\sigma_c \sim 4000$ Pa. The direction of the applied magnetic field in 100 Hz AC experiments was not observed to affect the critical stress, which suggests that the switching speed of the nano-MR fluid is less than 5 ms, and there was no lag between the AC induction field and particle tracking of that field.

Poddar et al. [51] provide a complete comparison of conventional (micron sized), nanoparticle, and hybrid particle MR fluids. The essential results are that MR fluids with micron sized particles exhibit superior critical stress, but poor sedimentation stability. Conversely, nano-MR fluids are found to have a much smaller critical stress, but much improved sedimentation stability. Hybrid systems offer a mix of both desirable qualities, where the actual performance may be tuned via the use of appropriate materials and sizes for the micro- and nanoparticles. The performance of an MR fluid formed by dispersion of our own magnetite/CNT composite in silicon oil differs from both the traditional MR and ferrofluid responses.

Magnetorheology of Novel Ferrofluids–CNT (FFCNT) Particle Suspensions

The ferrofluid–CNT (FFCNT) composite was dispersed in silicon oil (100 cSt PDMS oil, siloxane terminated, Gelest Inc., PA) at 5%, 10%, and 20% w/w fractions. Creep tests were performed in a parallel plate geometry, with a 40 mm anodized steel rotating plate, on an AR2000N rheometer (TA Instruments) (see Fig. 6). A custom designed MR fixture was employed to produce a uniform magnetic field normal to the sample [54].

Several creep experiments at constant shear stress were performed for each of three different stresses and volume fractions, and four different induction field strengths.

After each experiment, the sample was examined to ensure that the particles had not settled out of the suspension. The experiments were all conducted at 25°C, and maintained by a Peltier element below the MR fixture and a small fan that was used to intermittently cool the induction field coils after prolonged use. Figure 7 shows a consistent viscosity between samples within the field off regions. As expected, the rate of strain changes for each sample as a function of applied induction field, with the highest field strength resulting in the most diminished strain rate. Once the field is removed, the strain rate returns to its prefield value, regardless of the applied field intensity. These experiments were also repeated with other volume fractions of FFCNT composite. Figure 8 shows the viscosity shift as a function of increasing volume fractions. The greatest strain rate is observed at the lowest volume fraction, as is expected. The shift in zero field strain rate also appears to vary linearly with increasing volume fraction.

The shear rates for these creep experiments can be determined and used to evaluate the steady-state shear viscosity $\eta(\varphi, B, \sigma)$ as shown in Figs. 9–11. Apparently irrespective of applied field or particle mass fraction, these figures show that the FFCNT composite exhibits a critical stress between 20 Pa and 30 Pa. As the stress is progressively decreased the viscosity diverges and the fluids become increasingly solid-like. Continued shear thinning, albeit at a lesser rate, is expected as the shear stress increases,

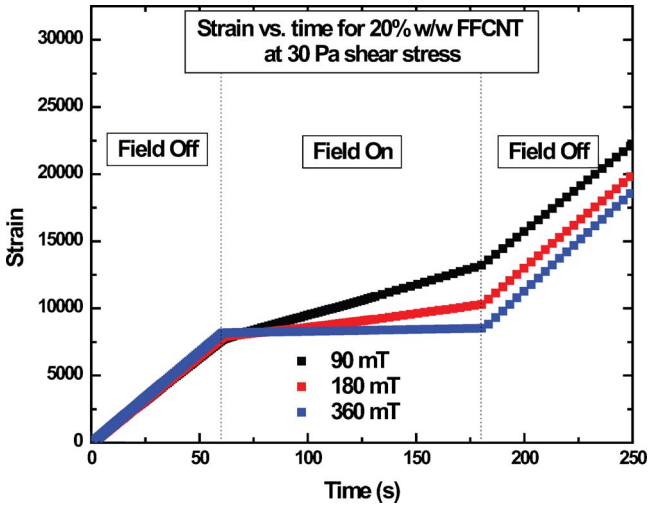

Fig. 7 Strain versus time for 20% w/w FFCNT, at 30 Pa shear stress, and three different induction fields

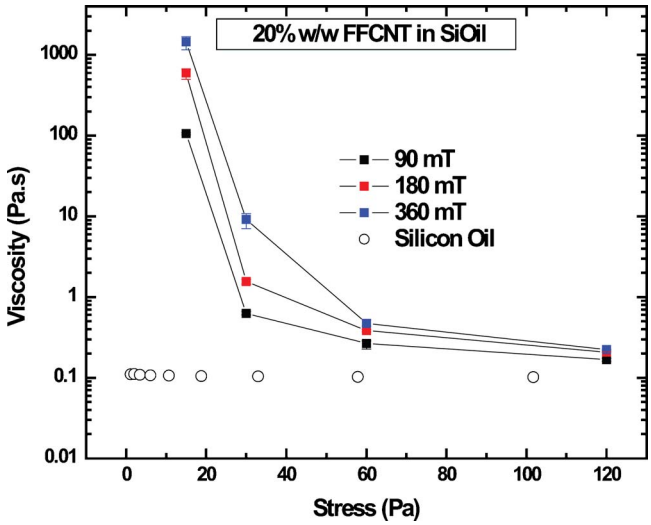

Fig. 9 Viscosity versus stress for 20% FFCNT at three induction fields

until the carrier viscosity is ultimately attained. As evidenced by the data, the rate of approach to this minimum is a function of both applied field and mass fraction. The 5% fraction reached the carrier viscosity (0.1 Pa s) by 60 Pa for all field strengths. The 20% and 10% samples exhibit a more gradual asymptotic approach at stresses $\sigma > 60$ Pa. Beyond 60 Pa, for all mass fractions, and applied induction fields, the test samples approached an infinite shear viscosity nearly equivalent to the carrier viscosity.

To model our CNT/Fe_3O_4 composite, it is assumed that the magnetic material lies within an external cylindrical coating of thickness ε, and is composed of randomly oriented superparamagnetic particles. This formation is a unique departure from the conventional carbonyl iron MR fluid particle, because the material composition allows for self-interaction in the absence of an applied external magnetic field. As such, the FFCNT may be considered to possess a combination of ferrofluid and MR particle properties. Due to the magnetic character of the hybrid, the aggregation parameter for our composite is likely to follow the ferrofluids model, as developed by Rosensweig [31], with an adjustment for the cylindrical shell geometry [35]. The greatest possible self-interaction field between two FFCNT cylinders would be 0.56 T, in the limit of favorable alignment of the superparamagnetic particles whose remnance magnetization is 0.56 T. Equation (4), which gives the aggregate parameter for ferrofluids can be modified for a cylindrical superparamagnetic shell of thickness ε, tube radius a, and composite length L and becomes

$$\lambda_m = \frac{\mu_0 MH[(\varepsilon + a)^2 - a^2]L\pi}{12k_B T\left(\ln\left(\frac{L}{2\varepsilon + 2a}\right) - 0.8\right)} \tag{11}$$

Calculating the value of this parameter for our magnetite–CNT composite gives $\lambda \cong 630$ and the self-interaction potential in the absence of external fields is therefore much closer to that seen in conventional MR fluids during actuation by an applied field. Based on this calculation, magnetic aggregation in the absence of an external field could be a partial explanation for the existence of micron-sized cylinders composed of multiple FFCNT threads. In MR fluids, $\lambda \gg 1$ leads to spontaneous agglomeration and sample-spanning structures upon application of an external field, and this leads to solidification of the entire fluid volume. In contrast,

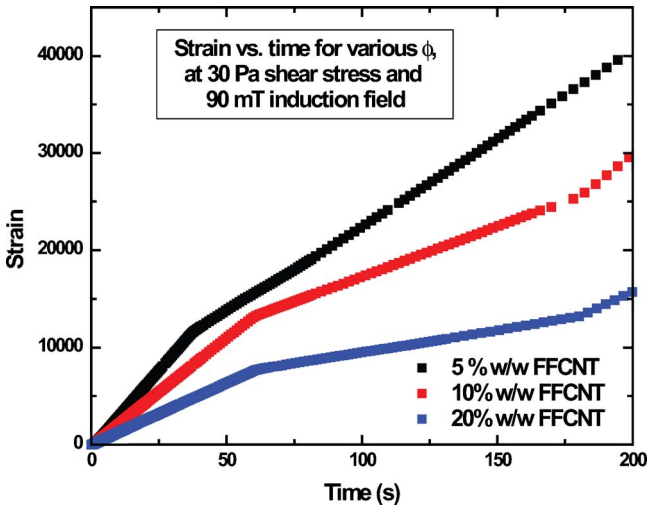

Fig. 8 Strain versus time for a 30 Pa shear stress and 90 mT induction field, at thee different mass fractions

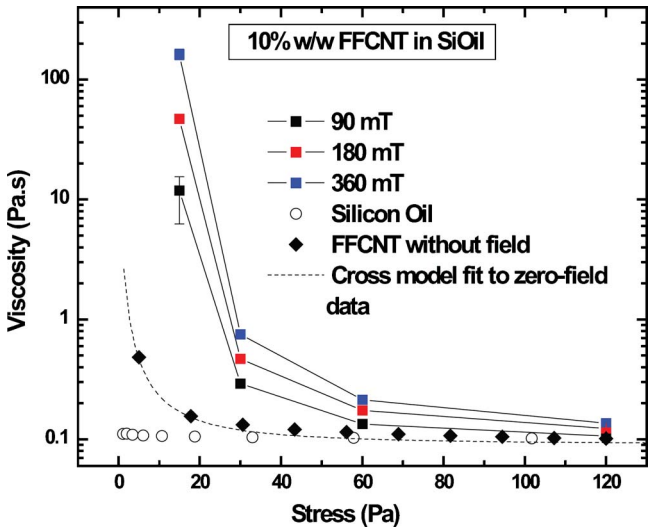

Fig. 10 Viscosity versus stress for 10% FFCNT at four different field strengths, with a Cross model fitting to the zero field data

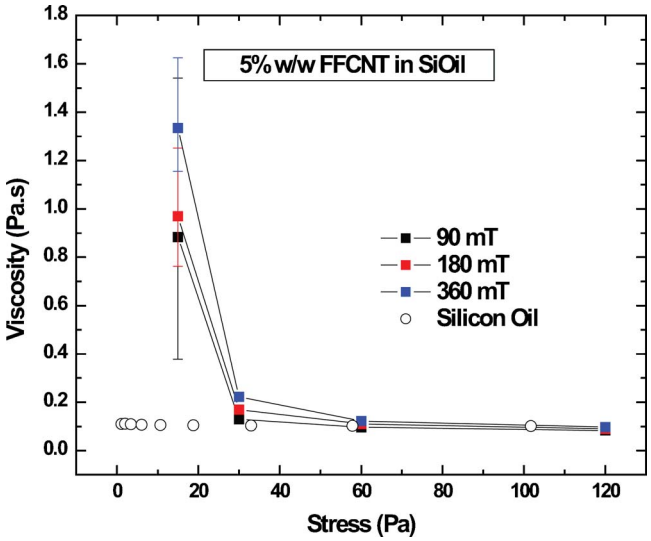

Fig. 11 Viscosity versus stress for 5% FFCNT at three induction fields

FFCNT aggregation induced by self-interaction appears to terminate after the combination of a sufficient number of individual threads.

The response to the imposed fields and shear stresses can also be quantified by considering an appropriate Mason number for each experimental data point. The Mason number as defined in Eq. (6) is not correctly formulated for a field responsive fluid composed of cylindrical, superparamagnetic components such as these FFCNT composites. Relying upon the relationship between Péclet and Mason numbers, and the coupling coefficient as defined in Eq. (11), a modified Mason number better suited for the FFCNT can be calculated in the form

$$\mathrm{Ma} = \frac{3\sigma(2\varepsilon + 2a)^2 \ln\left[\left(\frac{L}{2\varepsilon + 2a}\right) - 0.8\right]}{\mu_0 MH[(\varepsilon + a)^2 - a^2]} \tag{12}$$

Equation (12) demonstrates the appropriate interplay of hydrodynamic forces and those arising from the applied magnetic field, modified for the cylindrical geometry and superparamagnetic material. The calculated Mason number for these flows varies from 0.29 for a shear stress of 120 Pa and an induction field of 90 mT, to 0.009 for $\sigma = 15$ Pa and $\mu_0 H = 360$ mT. These values represent the two extremes in the range of Mason numbers for the experiments shown in Figs. 9–11. As expected, the highest values coincide with a Newtonian fluid-like response as observed when the fluid approaches an infinite shear-rate viscosity, and the lowest values coincide with the viscoplastic response observed at low shear stresses.

The fluid viscosities both below and above the critical stress, show a significant dependency on the magnitude of applied field and particle mass fraction. Likewise, the rate of shear thinning in the critical stress zone varies by orders of magnitude between different mass fractions.

The shear thinning behavior of CNT dispersions was also studied by Yang et al. [55]. Critical stresses for CNT volume fraction samples ranging from 0.04% to 0.42%, dispersed in low viscosity (4–6 cSt) poly-olefins, ranged from 0.04 Pa to 0.13 Pa, respectively. Flow experiments were performed, and the shear thinning behavior was fitted to the Cross model

$$\frac{\eta - \eta_\infty}{\eta_0 - \eta_\infty} = \frac{1}{1 + b\dot{\gamma}^P} \tag{13}$$

with values for P ranging from 0.560 to 0.772 in CNT suspensions. This expression also accurately describes the present zero-field rheological data as shown in Fig. 10. The range of data available preclude accurate determination of η_0, however the values of $b = 205$ and $P = 0.725$ are consistent with Ref. [55]. Further rheological characterization with our FFCNT suspensions demonstrated that a critical stress range still persists between 6 Pa and 12 Pa, even in the absence of a magnetic field.

Given the magnitude of the critical stress, and its persistence from 5% to 20% w/w, the critical stress appears to arise due to percolation of the cylindrical FFCNT composite. The range is amplified from the previously mentioned critical stress based on particle percolation due to the addition of superparamagnetic material that provides an additional strengthening interaction among the network elements. The lack of a stronger field dependence in the critical stress is expected for ferrofluids but not for a MR fluid in which the response is dominated by field-induced particle chaining. Conversely, the dependence of the zero shear-rate and infinite shear-rate viscosities on the induction field are expected for an MR fluid, but not found in a ferrofluid. It seems that this unique FFCNT composite exhibits attributes from both constituents, displaying a critical stress derived from a magnetically strengthened percolation network as well as field- and mass-fraction-dependent zero and infinite shear viscosities.

Final Remarks

We have reviewed the extensive literature on formulation techniques that exist to create magnetically-modified carbon nanotubes and their suitability for a wide variety of applications. Chemical and physical techniques have been utilized to introduce a diverse range of magnetic materials within CNTs, thus dramatically enhancing our ability to manipulate individual nanotubes, functionalize their surface, and induce self-assembly of complex nanostructures. Several of these techniques have been utilized to create novel MR fluids, and their viscometric properties have been demonstrated to enrich the range of rheological behavior that can be achieved with this class of non-Newtonian fluids. With the successful coupling of magnetic character to CNTs, it is possible to explore other interesting combinations of magnetism with unique CNT properties such as high electrical and thermal conductivity. Ongoing work includes combined magnetoelectric rheology, which capitalizes on the strong dielectrophoretic forces generated within the highly electrically conducting CNT, and the magnetic coating surrounding the CNT.

Acknowledgment

We would like to thank the Fannie and John Hertz Foundation for their support of this research, as well as the entire Non-Newtonian Fluids group within the Hatsopoulos Microfluids Laboratory at MIT.

Nomenclature

V_0 = sedimentation velocity (m/s)
ε = magnetic shell thickness (m)
L = aggregate length (m)
ρ_s = particle density (kg/m^3)
ρ_f = fluid density (kg/m^3)
g = gravitational acceleration (9.81 m/s^2)
a = particle, tube radius (m)
η = fluid viscosity (Pa s)
μ_0 = permeability of free space ($4\pi \times 10^{-7}$ N/A^2)
H = magnetic field (A/m)
χ = magnetic susceptibility
λ = ratio of magnetic aggregation force versus Brownian dispersion force

k_B = Boltzmann constant (1.38×10^{-23} J/K)
T = temperature (K)
Ma = Mason number, dimensionless ratio of hydrodynamic to magnetic forces
σ_c = critical yield stress (Pa)
σ = applied shear stress (Pa)
ϕ = particle volume fraction (v/v)
G = elastic modulus (Pa)

References

[1] Dresselhaus, M. S., Dresselhaus, G., and Jorio, A., 2004, "Unusual Properties and Structure of Carbon-Nanotubes," Annu. Rev. Mater. Res., **34**, pp. 247–278.
[2] Ajayan, P. M., Ebbesen, T. W., Ichihashi, T., Iijima, S., Tanigaki, K., and Hiura, H., 1993, "Opening Carbon Nanotubes With Oxygen and Implications for Filling," Nature (London), **362**(6420), pp. 522–525.
[3] Ajayan, P. M., and Iijima, S., 1993, "Capillarity-Induced Filling of Carbon Nanotubes," Nature (London), **361**(6410), pp. 333–334.
[4] Bao, J. C., Tie, C., Xu, Z., Suo, Z. Y., Zhou, Q. F., and Hong, J. M., 2002, "A Facile Method for Creating an Array of Metal-Filled Carbon Nanotubes," Adv. Mater., **14**(20), p. 1483.
[5] Leonhardt, A., Ritschel, A., Kozhuharova, R., Graff, A., Muhl, T., Huhle, R., Monch, I., Elefant, D., and Schneider, C. M., 2003, "Synthesis and Properties of Filled Carbon Nanotubes," Diamond Relat. Mater., **12**(3–7), pp. 790–793.
[6] Korneva, G., Ye, H. H., Gogotsi, Y., Halverson, D., Friedman, G., Bradley, J. C., and Kornev, K. G., 2005, "Carbon Nanotubes Loaded With Magnetic Particles," Nano Lett., **5**(5), pp. 879–884.
[7] Wu, H. Q., Wei, X. W., Shao, M. W., Gu, J. S., and Qu, M. Z., 2002, "Preparation of Fe–Ni Alloy Nanoparticles Inside Carbon Nanotubes via Wet Chemistry," J. Mater. Chem., **12**(6), pp. 1919–1921.
[8] Muhl, T., Elefant, D., Graff, A., Kozhuharova, R., Leonhardt, A., Monch, I., Ritschel, M., Simon, P., Groudeva-Zotova, S., and Schneider, C. M., 2003, "Magnetic Properties of Aligned Fe-Filled Carbon Nanotubes," J. Appl. Phys., **93**(10), pp. 7894–7896.
[9] Zhenyu Sun, Z. L., Wang, Y., Bursik, J., and Kadlecikov, M., 2005, "Fabrication and Characterization of Magnetic Carbon Nanotube Composites," J. Mater. Chem., **15**(42), pp. 4497–4501.
[10] Lafdi, K., Chin, A., Ali, N., and Despres, J. F., 1996, "Cobalt-Doped Carbon Nanotubes: Preparation, Texture, and Magnetic Properties," J. Appl. Phys., **79**(8), pp. 6007–6009.
[11] Rao, C. N. R., Sen, R., Satishkumar, B. C., and Govindaraj, A., 1998, "Large Aligned-Nanotube Bundles from Ferrocene Pyrolysis," Chem. Commun., **15**, pp. 1525–1526.
[12] Liu, S. W., Tang, X. H., Mastai, Y., Felner, I., and Gedanken, A., 2000, "Preparation and Characterization of Iron-Encapsulating Carbon Nanotubes and Nanoparticles," J. Mater. Chem., **10**(11), pp. 2502–2506.
[13] Liu, S. W., Zhu, J. J., Mastai, Y., Felner, I., and Gedanken, A., 2000, "Preparation and Characteristics of Carbon Nanotubes Filled With Cobalt," Chem. Mater., **12**(8), pp. 2205–2211.
[14] Banhart, F., Grobert, N., Terrones, M., Charlier, J. C., and Ajayan, P. M., 2001, "Metal Atoms in Carbon Nanotubes and Related Nanoparticles," Int. J. Mod. Phys. B, **15**(31), pp. 4037–4069.
[15] Zhang, X. X., Wen, G. H., Huang, S. M., Dai, L. M., Gao, R. P., and Wang, Z. L., 2001, "Magnetic Properties of Fe Nanoparticles Trapped at the Tips of the Aligned Carbon Nanotubes," J. Magn. Magn. Mater., **231**(1), pp. L9–L12.
[16] Georgakilas, V., Tzitzios, V., Gournis, D., and Petridis, D., 2005, "Attachment of Magnetic Nanoparticles on Carbon Nanotubes and Their Soluble Derivatives," Chem. Mater., **17**(7), pp. 1613–1617.
[17] Peng, D. L., Zhao, X., Inoue, S., Ando, Y., and Sumiyama, K., 2005, "Magnetic Properties of Fe Clusters Adhering to Single-Wall Carbon Nanotubes," J. Magn. Magn. Mater., **292**, pp. 143–149.
[18] Stoffelbach, F., Aqil, A., Jerome, C., Jerome, R., and Detrembleur, C., 2005, "An Easy and Economically Viable Route for the Decoration of Carbon Nanotubes by Magnetite Nanoparticles, and Their Orientation in a Magnetic Field," Chem. Commun., **36**, pp. 4532–4533.
[19] Choi, Y. C., Shin, Y. M., Lee, Y. H., Lee, B. S., Park, G. S., Choi, W. B., Lee, N. S., and Kim, J. M., 2000, "Controlling the Diameter, Growth Rate, and Density of Vertically Aligned Carbon Nanotubes Synthesized by Microwave Plasma-Enhanced Chemical Vapor Deposition," Appl. Phys. Lett., **76**(17), pp. 2367–2369.
[20] Bottini, M., Tautz, L., Huynh, H., Monosov, E., Bottini, N., Dawson, M. I., Bellucci, S., and Mustelin, T., 2005, "Covalent Decoration of Multi-Walled Carbon Nanotubes with Silica Nanoparticles," Chem. Commun. (Cambridge), **6**, pp. 758–760.
[21] Liu, J., Rinzler, A. G., Dai, H. J., Hafner, J. H., Bradley, R. K., Boul, P. J., Lu, A., Iverson, T., Shelimov, K., Huffman, C. B., Rodriguez-Macias, F., Shon, Y. S., Lee, T. R., Colbert, D. T., and Smalley, R. E., 1998, "Fullerene Pipes," Science, **280**(5367), pp. 1253–1256.
[22] Cao, H. Q., Zhu, M. F., and Li, Y. G., 2006, "Decoration of Carbon Nanotubes With Iron Oxide," J. Solid State Chem., **179**(4), pp. 1208–1213.
[23] Wu, H. Q., Cao, Y. J., Yuan, P. S., Xu, H. Y., and Wei, X. W., 2005, "Controlled Synthesis, Structure and Magnetic Properties of Alloy Nanoparticles Attached on Carbon Nanotubes," Chem. Phys. Lett., **406**(1–3), pp. 148–153.
[24] Gu, Y. and Li, D., 1999, "The Van Der Waals Interaction Between a Spherical Particle and Cylinder," J. Colloid Interface Sci., **217**(1), pp. 60–69.
[25] Kirsch, V. A., 2003, "Calculation of the Van Der Waals Force Between a Spherical Particle and an Infinite Cyinder," Adv. Colloid Interface Sci., **104**, pp. 311–324.
[26] Correa-Duarte, M. A., Grzelczak, M., Salgueirino-Maceira, V., Giersig, M., Liz-Marzan, L. M., Farle, M., Sierazdki, K., and Diaz, R., 2005, "Alignment of Carbon Nanotubes Under Low Magnetic Fields Through Attachment of Magnetic Nanoparticles," J. Phys. Chem. B, **109**(41), pp. 19060–19063.
[27] Pu, H. T., and Jiang, F. J., 2005, "Towards High Sedimentation Stability: Magnetorheological Fluids Based on CNT/Fe_3O_4 Nanocomposites," Nanotechnology, **16**(9), pp. 1486–1489.
[28] Razavian, S. M., Wenby, R. B., Fisher, T. C., and Meiselman, H. J., 1997, Biorheology, **34**, pp. 349–362.
[29] Klingenberg, D. J., 2001, "Magnetorheology, Applications and Challenges," AIChE J., **47**(2), pp. 246–249.
[30] Stanway, R., 2004, "Smart Fluids: Current and Future Developments," Mater. Sci. Technol., **20**(8), p. 931–939.
[31] Rosensweig, R. E., 1985, *Ferrohydrodynamics*, 2nd ed., Dover, Mineola, NY.
[32] Bossis, G., Lacis, S., Meunier, A., and Volkova, O., 2002, "Magnetorheological Fluids," J. Magn. Magn. Mater., **252**(1–3), pp. 224–228.
[33] Ginder, J. M., Davis, L. C., and Elie, L. D., 1996, "Rheology of Magnetorheological Fluids: Models and Measurements," Int. J. Mod. Phys. B, **10**(23–24), pp. 3293–3303.
[34] Tao, R., 2001, "Super-Strong Magnetorheological Fluids," J. Phys.: Condens. Matter, **13**(50), pp. R979–R999.
[35] Larson, R. G., 1999, *The Structure and Rheology of Complex Fluids*, Oxford University Press, New York.
[36] Rabinow, J., 1948, AIEE Trans., 67, p. 1308.
[37] Winslow, 1947, U.S. Patent No. 2,417,850.
[38] Wen, W. J., Huang, X. X., Yang, S. H., Lu, K. Q., and Sheng, P., 2003, "The Giant Electrorheological Effect in Suspensions of Nanoparticles," Nat. Mater., **2**(11), pp. 727–730.
[39] Promislow, J. H. E., Gast, A. P., and Fermigier, M., 1995, "Aggregation Kinetics of Paramagnetic Colloidal Particles," J. Chem. Phys., **102**(13), pp. 5492–5498.
[40] Fermigier, M., and Gast, A. P., 1992, "Structure Evolution in a Paramagnetic Latex Suspension," J. Colloid Interface Sci., **154**(2), pp. 522–539.
[41] Claracq, J., Sarrazin, J., and Montfort, J. P., 2004, "Viscoelastic Properties of Magnetorheological Fluids," Rheol. Acta, **43**(1), pp. 38–49.
[42] Ginder, J. M., 1998, "Behavior of Magnetorheological Fluids," MRS Bull., **23**(8), pp. 26–29.
[43] Rosensweig, R. E., Kaiser, R., and Miskolczy, G., 1969, "Viscosity of Magnetic Fluid in a Magnetic Field," J. Colloid Interface Sci., **29**(4), pp. 680–686.
[44] Rosensweig, R. E., 1996, "Negative Viscosity in a Magnetic Fluid," Science, **271**(5249), pp. 614–615.
[45] Rinaldi, C., and Zahn, M., 2002, "Effects of Spin Viscosity on Ferrofluid Duct Flow Profiles in Alternating and Rotating Magnetic Fields," J. Magn. Magn. Mater., **252**(1–3), pp. 172–175.
[46] Zahn, M., and Pioch, L. L., 1999, "Ferrofluid Flows in AC and Traveling Wave Magnetic Fields With Effective Positive, Zero or Negative Dynamic Viscosity," J. Magn. Magn. Mater., **201**, pp. 144–148.
[47] Kordonsky, W. I., Demchuk, S. A., 1996, "Additional Magnetic Dispersed Phase Improves the MR-Fluid Properties," J. Intell. Mater. Syst. Struct., **7**(5), pp. 522–525.
[48] Popplewell, J., Rosensweig, R. E., and Siller, J. K., 1995, "Magnetorheology of Ferrofluid Composites," J. Magn. Magn. Mater., **149**(1–2), pp. 53–56.
[49] Kormann, C., Laun, H. M., and Richter, H. J., 1996, "MR Fluids With Nano-Sized Magnetic Particles," Int. J. Mod. Phys. B, **10**(23–24), pp. 3167–3172.
[50] Chin, B. D., Park, J. H., Kwon, M. H., and Park, O. O., 2001, "Rheological Properties and Dispersion Stability of Magnetorheological (MR) Suspensions," Rheol. Acta, **40**(3), pp. 211–219.
[51] Poddar, P., Wilson, J. L., Srikanth, H., Yoo, J. H., Wereley, N. M., Kotha, S., Barghouty, L., and Radhakrishnan, R., 2004, "Nanocomposite Magneto-Rheological Fluids With Uniformly Dispersed Fe Nanoparticles," J. Nanosci. Nanotechnol., **4**(1–2), pp. 192–196.
[52] Phule, P. P., and Ginder, J., 1999, "Synthesis and Properties of Novel Magnetorheological Fluids Having Improved Stability and Redispersibility," Int. J. Mod. Phys. B, **12**, pp. 2019–2027.
[53] Chen, Z. Y., Tang, X., Zhang, G. C., Lin, Y., Ni, W., Zhu, Y. R., 1998, "A Novel Approach of Preparing Ultra Fine Magnetic Metallic Particles and Magnetorheology Measurements for Suspensions Containing These Particles," *Electro-rheological Fluids, Magneto-Rheological Suspensions and Their Applications*, M. Nakano and K. Koyama, eds., World Scientific, Singapore.
[54] Deshmoukh, S., 2006, Ph.D. thesis.
[55] Yang, Y., Grulke, E. A., Zhang, Z. G., and Wu, G. F., 2005, "Rheological Behavior of Carbon Nanotube and Graphite Nanoparticle Dispersions," J. Nanosci. Nanotechnol., **5**(4), pp. 571–579.